MATERIALS SCIENCE

Growth kinetics of single-walled carbon nanotubes with a (2*n*, *n*) chirality selection

Maoshuai He[1,2,3]*, Xiao Wang[2], Shuchen Zhang[4], Hua Jiang[5], Filippo Cavalca[6], Hongzhi Cui[3], Jakob B. Wagner[6], Thomas W. Hansen[6], Esko Kauppinen[5], Jin Zhang[4]*, Feng Ding[2,7]*

The growth kinetics play key roles in determining the chirality distribution of the grown single-walled carbon nanotubes (SWCNTs). However, the lack of comprehensive understandings on the SWCNT's growth mechanism at the atomic scale greatly hinders SWCNT chirality-selective synthesis. Here, we establish a general model, where the dislocation theory is a specific case, to describe the etching agent–dependent growth kinetics of SWCNTs on solid catalyst particles. In particular, the growth kinetics of SWCNTs in the absence of etching agent is validated by both in situ environmental transmission electron microscopy and ex situ chemical vapor deposition growth of SWCNTs. On the basis of the new theory of SWCNT's growth kinetics, we successfully explained the selective growth of (2*n*, *n*) SWCNTs. This study provides another degree of freedom for SWCNT controlled synthesis and opens a new strategy to achieve chirality-selective synthesis of (2*n*, *n*) SWCNTs using solid catalysts.

INTRODUCTION

Precise control of chirality during single-walled carbon nanotube (SWCNT) growth is crucial for applications in electronics, sensors, and devices (*1*). By means of controlling the carbon decomposition and developing catalysts, tangible progress has been achieved in the past two decades in chirality-selective synthesis of SWCNTs by chemical vapor deposition (CVD) (*2*–*11*). Although great experimental and theoretical efforts have been dedicated to the exploration of the SWCNT growth mechanism (*12*–*22*), our understanding on SWCNT's growth remains very limited, and rational experimental design for chirality-selective growth of SWCNTs is still scarce (*9*–*11*).

In general, the chirality distribution of the final SWCNT product is an interplay between the thermodynamics and kinetics of SWCNT growth (*11*). To address the growth kinetics, Ding *et al.* (*22*) proposed a screw dislocation model, in which the number of active sites at the interface between a SWCNT and the catalyst determines the SWCNT growth rate. Artyukhov *et al.* (*23*) later augmented the model by including the kinks created by thermal fluctuations on zigzag and armchair edges. Although the key conclusion of the dislocation theory, that the SWCNT growth rate is proportional to the number of active sites on the rim of the SWCNT, has been confirmed by many experimental observations (*2*, *3*, *20*) and applied to interpret the predominant growth of (n, $n-1$) SWCNTs, there are some contradictory reports (*24*, *25*). For example, it was confirmed by Raman spectroscopy (*26*) and transmission electron microscopy (TEM) (*25*) that the length of a SWCNT and its chiral angle have no correlations in some CVD experiments. To validate the screw dislocation theory, a precondition that SWCNT growth is limited by carbon atom incorporation into the SWCNT rim must be satisfied (*27*). Unfortunately, how to meet the conditions remains an uncharted territory, and a general model to describe the SWCNT growth kinetics, especially for those grown on recently thriving solid catalysts (*9*, *11*), is still pending.

In this present work, we propose a more comprehensive model for SWCNT growth kinetics, where the carbon concentration on a solid catalyst surface is balanced by the rate of precursor deposition, the rate of elimination by etching agents, and the rate of carbon incorporation into the active sites of the SWCNT. As a specific case of this general model, the screw dislocation theory is valid only when there is sufficient carbon etching agent during SWCNT growth. When there is limited etching agent, SWCNT growth is governed by the ratio of the exposed catalyst surface area to the tube diameter, as also verified by in situ environmental TEM (ETEM) characterizations. In such a regime, precise control of the concentration of the etching agent gradually deactivates the growth of SWCNTs with fewer active sites and allows only the growth of (2*n*, *n*) SWCNTs with the most active sites.

RESULTS

Theoretical model

During catalytic CVD growth of a SWCNT, several elementary reactions on the catalyst surface—carbon source decomposition, the elimination of carbon atoms by etching agents, carbon atom diffusion on the catalyst surface, and the incorporation of carbon atoms from the catalyst surface into the wall of the SWCNT—are involved in all the three key stages of SWCNT growth: Graphitic cap nucleation, tube wall elongation, and growth termination. It is broadly recognized that the nucleation of SWCNT on a catalyst surface controls the chirality of the SWCNT (*28*, *29*). Previous theoretical analysis and experimental studies have shown that the chirality control during SWCNT nucleation can be achieved using designed solid catalysts to template the nucleation of the SWCNTs, and many solid catalysts with high melting points were designed to grow SWCNTs with specific chiralities (*9*, *11*). In this study, we focus the kinetics of tube wall elongation and growth termination and their effects on the SWCNT chirality selection. Depending on the state of the catalyst, SWCNT growth may follow either vapor-solid-solid (VSS) or vapor-liquid-solid (VLS) mechanisms. During the SWCNT VLS growth, the shape of a liquid catalyst may fluctuate quickly and, therefore,

[1]State Key Laboratory of Eco-Chemical Engineering, Ministry of Education, Taishan Scholar Advantage and Characteristic Discipline Team of Eco Chemical Process and Technology, College of Chemistry and Molecular Engineering, Qingdao University of Science and Technology, Qingdao 266042, China. [2]Center for Multidimensional Carbon Materials, Institute for Basic Science, UNIST-gil 50, Ulju-gun, Ulsan 44919, Republic of Korea. [3]School of Materials Science and Engineering, Shandong University of Science and Technology, Qingdao 266590, China. [4]College of Chemistry and Molecular Engineering, Peking University, Beijing 100871, China. [5]Department of Applied Physics, Aalto University School of Science, P.O. Box 15100, FI-00076 Aalto, Finland. [6]Center for Electron Nanoscopy, Technical University of Denmark, DK-2800 Kongens Lyngby, Denmark. [7]School of Materials Science and Engineering, Ulsan National Institute of Science and Technology, Ulsan 44919, Republic of Korea.
*Corresponding author. Email: hemaoshuai@qust.edu.cn (M.H.); jinzhang@pku.edu.cn (J.Z.); gniding@gmail.com (F.D.)

is hard to be modeled. In contrast, during the elongation process of a SWCNT in VSS growth, the shape of the catalyst is quite stable, and the carbon concentration evolution on the catalyst surface can be well addressed. On the surface of a solid catalyst particle, the variation of the carbon atoms can be written as

$$A \times dc/dt = (\alpha \times A \times P) - (\beta \times A \times c) - (\gamma \times c \times N_{ACT}) \quad (1)$$

where α and γ are constants, A is the active surface area of catalyst that is accessible to the feedstock molecules during the SWCNT growth, c is the concentration of carbon atoms on the catalyst surface, and P is the pressure of the feedstock gas. β depends on the concentration of the etching agent, and β = 0 if there is no etching agent in SWCNT growth. The first term on the right side of the equation represents the carbon atoms released by feedstock dissociation, which is proportional to the product of the active catalyst surface and the pressure of the carbon feedstock; the second term originates from the elimination of carbon atoms from the catalyst surface by the etching agents, which is proportional to the number of accessible carbon atoms on the catalyst surface, i.e., the product of the accessible area of the catalyst surface and the concentration of carbon atoms on the catalyst surface (*9*, *11*, *30*, *31*); and the third term counts the consumption of carbon atoms during the SWCNT growth, where the rate of carbon attachment is proportional to the product of the number of active sites at the SWCNT-catalyst interface, N_{ACT}, and c.

For the steady state of SWCNT growth ($dc/dt = 0$), the concentration of carbon atoms on the catalyst surface is

$$c = \frac{\alpha P}{\beta + \gamma \frac{N_{ACT}}{A}} \quad (2)$$

In a situation where SWCNT growth occurs in an environment with sufficient etching agent, most carbon atoms released by the decomposition of the feedstock are removed by the etching agents or $\beta >> \gamma \frac{N_{ACT}}{A}$, and Eq. 2 becomes

$$c = \frac{\alpha}{\beta} P \quad (3)$$

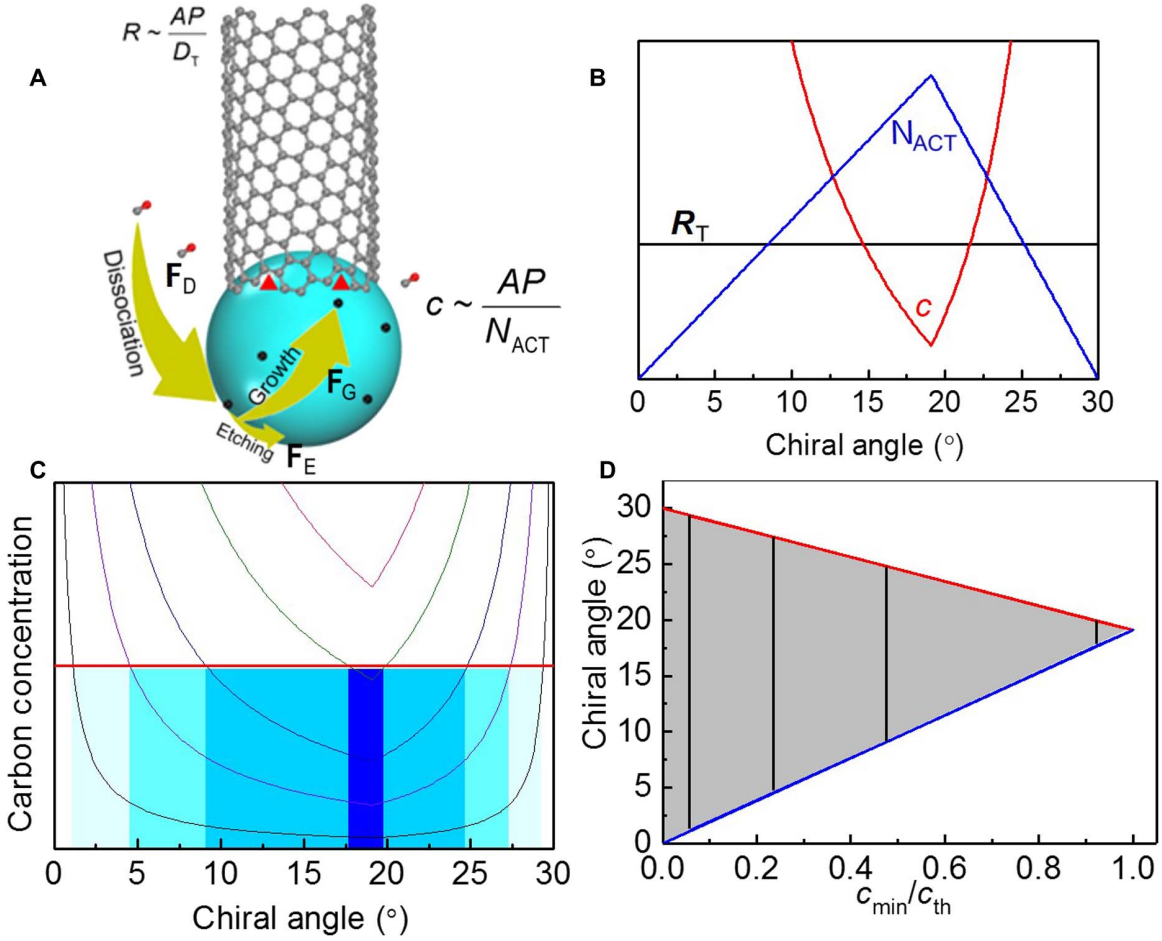

Fig. 1. SWCNT growth mode without enough etching agents. (**A**) Growth model for SWCNT growth in the absence of sufficient etching agents. (**B**) In the growth regime, the SWCNT growth rate (R_T), active sites for carbon incorporation (N_{ACT}), and catalyst surface carbon concentration (c) plots against the tube chiral angle. (**C**) Carbon concentration as a function of the SWCNT chiral angle at different fluxes of carbon deposition. The threshold carbon concentration (c_{th}) for catalyst encapsulation is indicated by the red line. (**D**) The chirality-selective growth of SWCNTs as a function of c_{min}/c_{th}, where the dark zone indicates the SWCNTs can survive under different carbon fluxes.

This means that the concentration of carbon atoms on the catalyst surface, c, is independent of the specifications of the catalyst and the SWCNT. Under these circumstances, the SWCNT growth rate is

$$R \sim c \times \frac{N_{ACT}}{D_T} \sim P \times \frac{N_{ACT}}{D_T} \quad (4)$$

where D_T is the diameter of the SWCNT and $\frac{N_{ACT}}{D_T}$ is the concentration of active sites at the rim of the SWCNT. According to the screw dislocation theory, the active sites are the armchair-like sites for SWCNT VLS growth (*22*), but only kink sites are active in the SWCNT VSS growth (*23*). Equation 4 shows that the conclusion of the screw dislocation theory (*22*, *23*) is valid only if there is sufficient etching agent during the SWCNT growth, which ensures that most of the carbon atoms on the catalyst surface are etched away or the carbon flux of etching is substantially higher than that of growth, $\mathbf{F}_E >> \mathbf{F}_G$ (fig. S1). Under such a circumstance, the concentration of carbon atoms on the catalyst surface, c, is independent of the SWCNT chiral angle, and the growth rate is proportional to the number of active sites, N_{ACT}.

Experimentally, H_2 (*9*, *11*, *30*), H_2O (*31*), O_2 (*30*), or CO_2 (*32*) has been used as an etching agent, and each of them can efficiently remove carbon atoms from the catalyst surface and maintain a clean catalyst particle surface for SWCNT growth. In contrast, if there is no or limited etching agent, then the second term in Eq. 1 will be dominating, and the carbon concentration on the catalyst surface during the SWCNT's steady-state growth becomes

$$c = \frac{\alpha}{\gamma} \frac{AP}{N_{ACT}} \quad (5)$$

which depends on the number of active sites of the SWCNT and the size of the catalyst particle. In this regime, the growth rate of a SWCNT is

$$R \sim c \times \frac{N_{ACT}}{D_T} \sim \frac{AP}{D_T} \quad (6)$$

It shows that the growth rate of a SWCNT is proportional to the ratio of the accessible area of the catalyst surface to the tube diameter (A/D_T) and the feedstock pressure (P) but independent of the number of active sites of at the interface between the SWCNT and the catalyst (N_{ACT}).

Equations 5 and 6 indicate another regime of SWCNT growth, where there is no sufficient etching agent and most of the carbon atoms

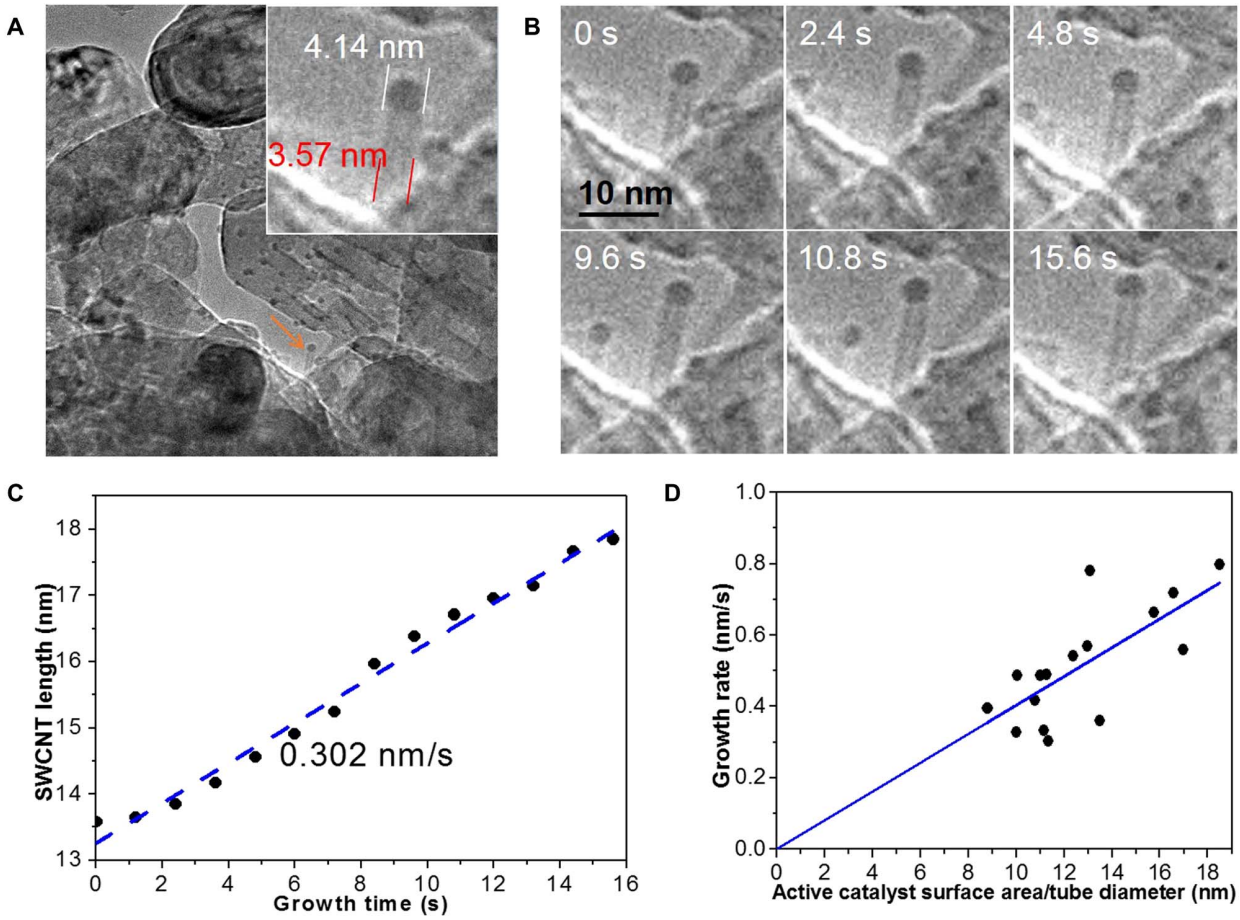

Fig. 2. SWCNT growth rate. (**A**) Snapshot of a SWCNT (named #1 in our samples) and its magnified image (inset) taken during its growth. (**B**) Six ETEM images (extracted from movie S1) of the tube taken at different times during growth. (**C**) SWCNT length plotted as a function of growth time shows a constant growth rate. (**D**) SWCNT growth rate plots as a function of active catalyst surface area–to–tube diameter ratio.

from the carbon feedstock decomposition must either stay on the surface of the catalyst or be incorporated into the SWCNT wall, as schematically illustrated in Fig. 1A. In such a regime, because of the lack of etching agent ($\mathbf{F}_E << \mathbf{F}_G$), the feedstock decomposition cannot be balanced by carbon etching. Consequently, the carbon concentration on the catalyst surface, c, is SWCNT structure dependent and is inversely proportional to N_{ACT} (Fig. 1B). According to the VSS SWCNT growth model, the ($2n$, n) SWCNTs, which have a chiral angle of 19.1°, have the maximum density of active kink sites at the interface of the SWCNT and the catalyst. As a consequence, the carbon concentration on the catalyst surface is smallest if the chirality of the growing SWCNT is ($2n$, n).

As shown in the above model of SWCNT growth, the carbon concentration on the catalyst surface, which is determined by N_{ACT}, should have an impact on the lifetime of an SWCNT's growth. It is widely known that the termination of SWCNT growth is mainly caused by the encapsulation of the catalyst particle by graphitic carbon (*33*, *34*). Catalyst particle encapsulation requires the carbon concentration on the catalyst surface exceed a threshold value, c_{th}. Figure 1C plots the carbon concentration as a function of the SWCNT's chiral angle (Eq. 5) at different fluxes of carbon deposition ($\mathbf{F}_D$). It shows that a catalyst particle with a SWCNT of less active sites has a higher carbon concentration on its surface and, thus, the SWCNT growth might easily be terminated. With the increase in the flux of carbon deposition, $\mathbf{F}_D$, more and more growing SWCNTs with fewer active sits are deactivated, resulting in the survival of SWCNTs with a narrower chiral angle distribution around that of ($2n$, n) SWCNTs, 19.1°. Using the threshold concentration shown in Fig. 1C, a diagram of SWCNT growth is deduced (Fig. 1D). Obviously, the higher the carbon deposition flux, the narrower the chirality distribution of the surviving SWCNTs around ($2n$, n).

As shown in Eq. 5, carbon atom concentration on the catalyst surface is geometry (A) dependent. So, to achieve the selective growth of the ($2n$, n) SWCNTs using solid catalysts, the catalyst particles must have similar sizes and accessible surface area. Experimentally, catalyst size control is a critical step in chirality-selective growth of SWCNTs, and most of the previous experiments producing the chirality-selective SWCNTs are realized with uniformed catalyst sizes (*11*). So, when discussing chirality-selective SWCNT growth, the parameter regarding the geometrical shape of the catalyst particle is considered as a constant, and therefore, the c is only considered as a function of P and N_{ACT}. As a result, it is reasonable to consider c_{min} as an experimental constant.

Experimental results

The above model shows that only SWCNTs with more active sites can survive at a large carbon flux when there is no etching agent. On the basis of the analysis, a new mechanism for selective growth of ($2n$, n) SWCNTs is thus proposed by increasing the carbon flux and greatly decreasing the concentration of the etching agent. When the growing SWCNT has very few active sites, the concentration of carbon on the catalyst, c, is higher than c_{th}, which will lead to the nucleation of a graphitic carbon around the catalyst particle and the termination of the SWCNT growth (*30*, *31*, *35*). Therefore, to avoid growth termination in such a regime and to study the SWCNT growth kinetics, a low-temperature CVD SWCNT growth using a low-pressure feedstock is required (*35*).

With the aim to investigate SWCNT growth kinetics in the feedstock-limited regime, in situ ETEM was first used to monitor the steady growth of SWCNTs at 700°C with CO as the carbon feedstock on an MgO support Co catalyst (*36*). Such a high-vacuum environment is almost free of etching agents because the generation of oxidation etchants, CO_2 from CO disproportionation or O desorption from

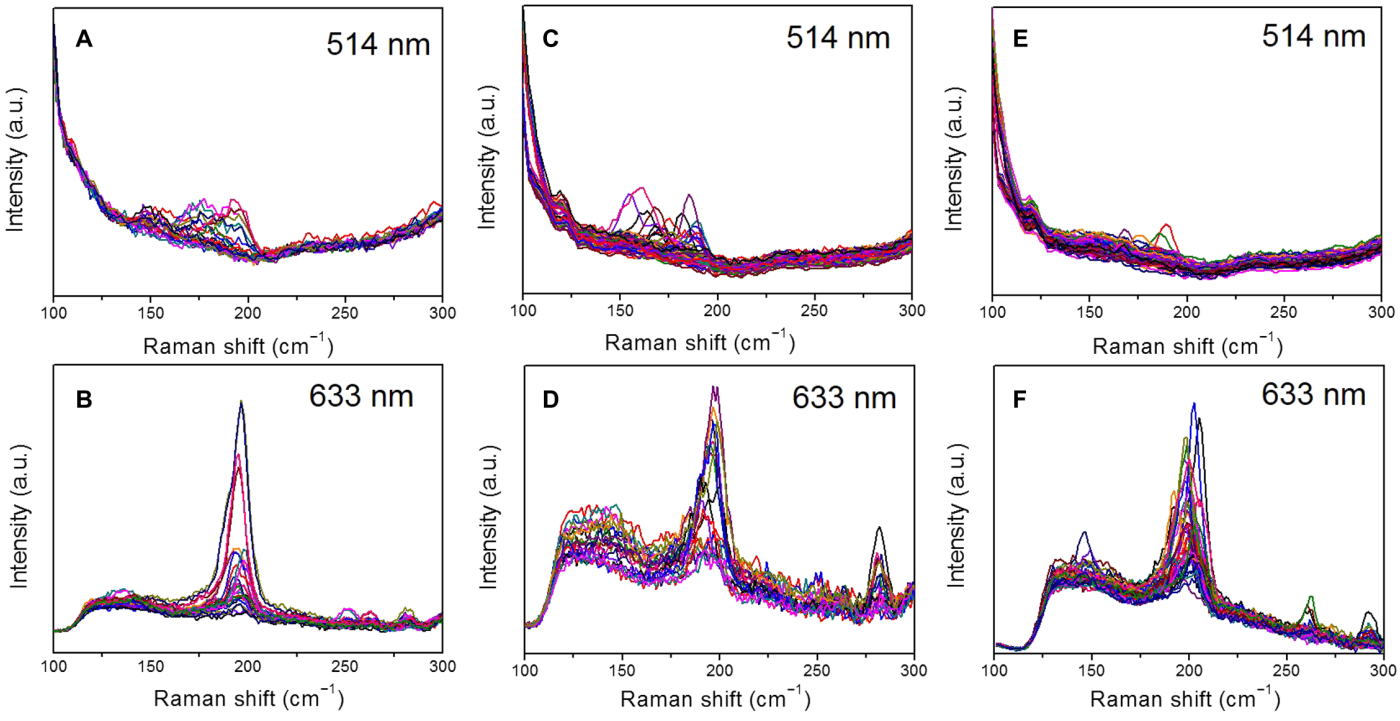

Fig. 3. Raman spectra of carbon nanotubes grown on Co nanoparticles with different CO flow fluxes. (**A** and **B**) Thirty standard cubic centimeters per minute (sccm), (**C** and **D**) 40 sccm, and (**E** and **F**) 50 sccm. The excitation laser wavelengths are all labeled. a.u., arbitrary units.

support, is greatly suppressed. Movie S1 shows the nucleation and growth of many SWCNTs in the field of observation. Every SWCNT contains a Co nanoparticle on its top end, a typical feature of tip growth. Figure 2A shows one SWCNT (denoted as #1) with a diameter of ~3.57 nm and a catalyst particle of ~4.14 nm. By following the elongation of the SWCNT (Fig. 2B), it is indicated that the length of SWCNT increases linearly with time at a growth rate of 0.302 nm/s (Fig. 2C).

DISCUSSION

Linear growth behavior was also observed for another 15 SWCNTs, which are marked and shown in fig. S2. The growth rates, diameters of the SWCNTs and the catalyst particles, and the active catalyst areas (defined as the area of the catalyst surface exposed to the feedstock) of the 16 SWCNTs are listed in table S1. Figure S3 (A and B) shows that an SWCNT's growth rate, R, is independent on its diameter, D_T, or the size of the catalyst particle, D_C. In contrast, by plotting R against A/D_T according to Eq. 6 (Fig. 2D), a strong linear relationship between the growth rate and the active catalyst surface/tube diameter ratio is shown. The findings indicate that all the carbon atoms from decomposition, whose number is proportional to the active surface of the catalyst particle, become a part of the SWCNT whatever the number of active sites in the SWCNT-catalyst interface. In agreement with our proposed model, the growth behavior depends on the sizes of the SWCNT and the catalyst only. This is in sharp contrast to the screw dislocation model (*22*, *23*), in which the growth rate is proportional to the number of active sites.

The absence of an etching agent leads to a high carbon concentration on the surface of a catalyst particle with an SWCNT having fewer active sites. To verify the model and achieve SWCNTs with a narrow chirality distribution, it is necessary to increase the carbon deposition flux while minimizing the amount of possible weak oxidation etchants. Consequently, Co nanoparticles deposited onto a quartz substrate were applied to synthesize SWCNTs under ambient pressure with different carbon fluxes. Figure S4 shows the scanning electron microscopy (SEM) of carbon nanotubes grown on Co catalysts using Ar-diluted CO as the carbon source. Raman spectra acquired on the three samples using two excitation lasers (514 and 633 nm) are depicted in Fig. 3. On the

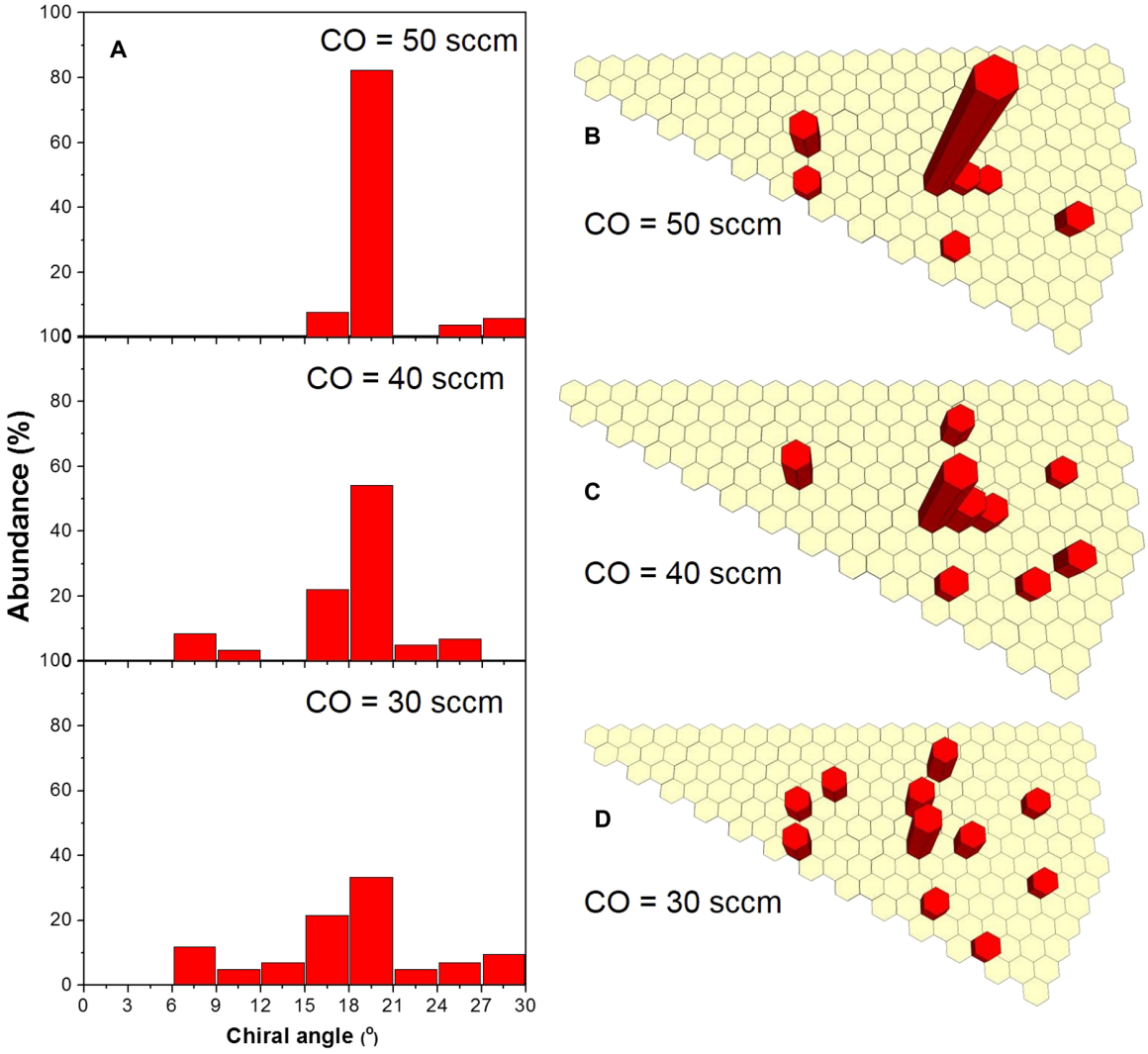

Fig. 4. SWCNT chirality selectivity as a function of CO flow rate. (**A**) Chiral angle distributions of SWCNTs grown on quartz-supported Co nanoparticles with different flow rates of CO at 650°C. Chirality map of SWCNTs grown with (**B**) 50 sccm CO, (**C**) 40 sccm CO, and (**D**) 30 sccm CO.

basis of the Kataura plot, the chirality distributions of the SWCNTs grown with different CO fluxes are deduced and shown in fig. S5 and table S2.

The growth results can be well explained by the proposed model in the regime of carbon feedstock-controlled growth. As can be seen from Fig. 4, with the increase in CO flow rate, the selectivity to (2*n*, *n*) SWCNTs increases sharply from 33.4 to 82.3%. The best selectivity is achieved in the presence of the highest CO flow rate [50 standard cubic centimeters per minute (sccm); Fig. 4, A and B]. In the growth regime, under a relatively low carbon flux (30 sccm), only SWCNTs with fewer active sites (near zigzag species) for carbon incorporation are deactivated by carbon encapsulation, resulting in the growth of SWCNTs with relatively wide chirality distribution (Fig. 4D), although the most abundant species still are (2*n*, *n*) SWCNTs, such as (12, 6), (8, 4), and (16, 8). Gradually increasing the carbon flow rate narrows the chirality distribution by deactivating the growth of more SWCNTs with fewer kinks (Fig. 4, B and C). In particular, with a 50-sccm CO flow, the carbon concentrations on most catalyst particle surfaces exceed c_{th}, and mainly those Co particles growing (2*n*, *n*) SWCNTs maintain their activities, accounting for the high-selectivity growth of (2*n*, *n*) SWCNTs. Note that besides the SWCNT growth kinetics demonstrated in this work, the chirality distribution of grown SWCNTs may also be affected by the symmetry of the solid catalyst particle and the diameter distribution of the prepared catalysts (*37*). For example, SWCNTs with five- or sevenfold symmetry, such as the (14, 7) or (10, 5) ones, are rarely observed in the final products due to the lack of catalyst surface with this symmetry, and the abundance of the (*n*, *m*) other than (12, 6) could be different because of the strong correlation between the diameters of the catalyst particle and the SWCNT grown on it.

For each catalyst, the SWCNT growth window is unique and generally not wide. No SWCNT growth was observed with low CO flow using quartz-supported Co nanoparticles. To observe the switching between two regimes of SWCNT growth as indicated by the theoretical model, the $Co_xMg_{1-x}O$ catalyst powder was dispersed onto a porous Si_3N_4 grid and loaded for ambient CVD growth with 1% CO, which was diluted by He. Typical SEM image and TEM image of as-prepared SWCNTs are respectively shown in Fig. 5 (A and B). On the basis of the nanobeam electron diffraction characterizations on 89 SWCNTs, the chiral angle distribution of the obtained SWCNTs was obtained. Near-armchair SWCNT species were obtained (Fig. 5C), suggesting that SWCNT growth on such a catalyst follows the screw dislocation model in the growth regime. The generation of weak etching agents, arising from porous MgO desorption or CO disproportionation, is responsible for the growth of near-armchair species, following the screw dislocation model.

This new mechanism is also applicable to the chirality-controlled growth of (2*n*, *n*) SWCNTs on Mo_2C catalyst reported recently (*11*). Experimentally, the best selective growth of (2*n*, *n*) SWCNTs was achieved in the absence of any etching agent (e.g., H_2 flow becomes zero) and with a high feedstock concentration. Table S3 presents the chirality distributions of SWCNTs synthesized with different ethanol-to-H_2 (E:H) ratios in the feedstock. From fig. S6, we can see that (i) a high concentration of H_2 in the gas phase (E:H, 100:200) results in a wide SWCNT chirality distribution; (ii) decreasing the H_2 concentration leads to a narrower distribution of the SWCNTs around (2*n*, *n*) SWCNTs; and (iii) under the optimal growth conditions (E:H, 100:0), the low concentration of etching agents in the vapor phase leads to the highest selection of (12, 6) tubes up to 87.0%. The role of the etching agent in the selective growth of SWCNTs can be perfectly explained on the basis of the new mechanism. When the H_2 concentration is very high, all the SWCNTs have the same probability of having their growth terminated, and therefore, the low chirality selectivity is dominated by the fast growth of (2*n*, *n*) SWCNTs. Gradually decreasing the H_2 concentration leads to a change of growth regime and a fast increase in the carbon concentration on the catalyst surface for SWCNTs with few active sites. Consequently, when *c* exceeds c_{th}, tube growth will be terminated, and eventually, only a few SWCNTs whose chiral angles are close to that of (2*n*, *n*), 19.1°, can survive under a high carbon flux.

Our theoretical analysis and in situ/ex situ experiments unambiguously prove that enough etching agent in the environment is a precondition of the screw dislocation theory for SWCNT growth and that when there is no etching agent, the growth rate of a SWCNT is structure independent. As revealed by the ETEM characterizations, the growth rate is proportional to the ratio of the exposed catalyst surface area to the tube diameter. This new understanding is a complement to the previous mechanism of SWCNT growth and offers a new degree of freedom to control SWCNT chirality by experimental design. The agreement between the new mechanism of SWCNT's chirality selectivity and the experimental results clarifies the mystery of SWCNT chirality-selective growth achieved without sufficient etching agent. Together with other strategies of chirality selectivity in SWCNT growth, such as seeded growth, epitaxial growth, and catalyst size control, the large-scale production of SWCNTs with any defined chirality might be achieved soon.

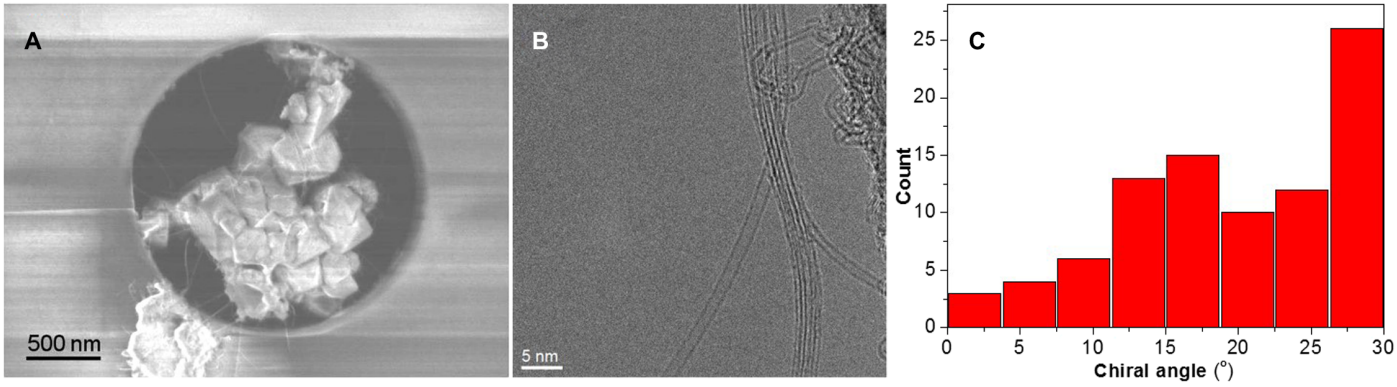

Fig. 5. Near-armchair SWCNT growth on $Co_xMg_{1-x}O$ catalyst. (**A**) SEM of SWCNTs grown on $Co_xMg_{1-x}O$ catalyst with 1% diluted CO at 700°C by ambient CVD. (**B**) TEM image of SWCNTs. (**C**) Chirality distribution of SWCNTs determined by nanobeam electron diffraction.

MATERIALS AND METHODS

Preparation and characterizations of the $Co_xMg_{1-x}O$ catalyst

The catalyst was prepared by atomic layer deposition (ALD) (*5*, *38*). A porous MgO support obtained from the thermal decomposition of magnesium carbonate hydroxide hydrate was loaded into an F120 ALD reactor. After annealing in N_2 at 400°C for 5 hours, cobalt(III) acetylacetonate (98%; Sigma-Aldrich) evaporated at 190°C passed through the MgO bed and the precursor deposition lasted 6 hours. Last, the catalyst was flushed with N_2 and annealed in air at 450°C for another 4 hours. All the processes were kept at a low pressure (60 to 100 mbar) (*36*, *39*).

In situ ETEM studies of SWCNT growth on the $Co_xMg_{1-x}O$ catalyst

In situ CO CVD was performed on an aberration-corrected FEI Titan 80-300FEG ETEM operated at 300 kV (*6*, *35*, *36*). The $Co_xMg_{1-x}O$ catalyst (*36*) was collected on a bare Au grid and mounted in a tantalum double-tilt heating holder. After insertion into the TEM chamber and heating to 700°C in Ar, CO was introduced to maintain a pressure of 9.5 mbar. After stabilization, the formation of Co nanoparticles and the growth of carbon nanotubes were monitored.

Growth and characterizations of SWCNTs grown on the $Co_xMg_{1-x}O$ catalyst

The $Co_xMg_{1-x}O$ catalyst powder was dispersed onto an Si_3N_4 TEM grid (DuraSIN mesh) and loaded into a horizontal CVD reactor (quartz tube inner diameter, 40 mm). After being heated to 700°C in He flow, diluted CO in He (5 sccm CO + 495 sccm He) was switched in, and the growth lasted 1 hour. After cooling down, as-prepared SWCNTs were characterized by SEM (JSM-7500F, JEOL) and TEM (2200FS, JEOL) operated at 80 kV. The electron diffraction patterns of individual SWCNTs were acquired with the same TEM, and the chiral angle was assigned on the basis of a calibration-free method (*40*, *41*).

Growth and characterizations of SWCNTs on quartz-supported Co catalyst by ambient pressure CO CVD

To realize the SWCNT horizontal array on quartz at 650°C, the precursors, $CoSO_4$/ethanol solution (0.1 mM/liter), were predispersed on quartz substrate and annealing in air at 400°C for 5 hours. The substrate with Co precursors was then loaded into the tube furnace and flushed with 300 sccm Ar. When the temperature reached 650°C, 100 sccm H_2 was introduced to reduce the catalysts for 10 min. After reducing, CO with different flow fluxes, 30, 40, and 50 sccm, was introduced to replace H_2 and grow carbon nanotubes for 15 min. The as-produced SWCNTs were transferred onto SiO_2 substrates for Raman characterizations with two laser wavelengths: 514 and 633 nm. The abundance of SWCNTs with different chiralities was determined from the numbers of acquired radial breathing modes.

Characterization of SWCNT growth on Mo_2C catalyst by Raman spectroscopy

Preferential synthesis of (12, 6) nanotubes was achieved on sapphire substrate with Mo_2C as the catalyst. The detailed procedure has been reported elsewhere (*11*). Briefly, after the reduction of MoO_3 catalyst, the catalyst was heated to 850°C in Ar. A flux of 100 sccm Ar passing through an ethanol bubbler mixed with H_2 was then introduced into the CVD reactor for growing SWCNTs. The respective H_2 flow rate was set to be 0, 10, 50, 100, and 200 sccm for five experimental runs. The growth run lasted 15 min. Raman spectroscopy (HORIBA HR800 equipped with four lasers of different wavelengths: 488, 514, 633, and 785 nm) was performed to estimate the chirality distribution of SWCNTs transferred onto SiO_2 substrates.

SUPPLEMENTARY MATERIALS

Supplementary material for this article is available at http://advances.sciencemag.org/cgi/content/full/5/12/eaav9668/DC1

Fig. S1. Model of SWCNT growth following a screw dislocation theory.
Fig. S2. Investigated SWCNTs (marked with arrows) and calculated growth rates.
Fig. S3. SWCNT growth rate plots against tube diameter and catalyst size.
Fig. S4. SEM images of carbon nanotubes grown on quartz-supported Co catalyst.
Fig. S5. Chirality distribution histograms of SWCNTs grown on Co particles with different CO fluxes.
Fig. S6. Chirality evolution and distribution of SWCNTs grown on Mo_2C.
Table S1. Growth rates and corresponding parameters of SWCNTs and catalysts for 16 different SWCNTs.
Table S2. (*n*, *m*) populations of SWCNTs grown on Co catalyst using different flow rates of CO.
Table S3. Chirality distribution of SWCNTs grown on Mo_2C using different ratios of ethanol and H_2.
Movie S1. In situ observation of SWCNT growth.

REFERENCES AND NOTES

1. R. H. Baughman, A. A. Zakhidov, W. A. de Heer, Carbon nanotubes—The route toward applications. *Science* **297**, 787–792 (2002).
2. S. M. Bachilo, L. Balzano, J. E. Herrera, F. Pompeo, D. E. Resasco, R. B. Weisman, Narrow (*n*,*m*)-distribution of single-walled carbon nanotubes grown using a solid supported catalyst. *J. Am. Chem. Soc.* **125**, 11186–11187 (2003).
3. S. Maruyama, Y. Miyauchi, Y. Murakami, S. Chiashi, Optical characterization of single-walled carbon nanotubes synthesized by catalytic decomposition of alcohol. *New J. Phys.* **5**, 149.141–149.112 (2003).
4. X. Li, X. Tu, S. Zaric, K. Welsher, W. S. Seo, W. Zhao, H. Dai, Selective synthesis combined with chemical separation of single-walled carbon nanotubes for chirality selection. *J. Am. Chem. Soc.* **129**, 15770–15771 (2007).
5. M. He, A. I. Chernov, P. V. Fedotov, E. D. Obraztsova, J. Sainio, E. Rikkinen, H. Jiang, Z. Zhu, Y. Tian, E. I. Kauppinen, M. Niemelä, A. O. I. Krause, Predominant (6,5) single-walled carbon nanotube growth on a copper-promoted iron catalyst. *J. Am. Chem. Soc.* **132**, 13994–13996 (2010).
6. M. He, H. Jiang, B. Liu, P. V. Fedotov, A. I. Chernov, E. D. Obraztsova, F. Cavalca, J. B. Wagner, T. W. Hansen, I. V. Anoshkin, E. A. Obraztsova, A. V. Belkin, E. Sairanen, A. G. Nasibulin, J. Lehtonen, E. I. Kauppinen, Chiral-selective growth of single-walled carbon nanotubes on lattice-mismatched epitaxial cobalt nanoparticles. *Sci. Rep.* **3**, 1460 (2013).
7. H. Wang, B. Wang, X.-Y. Quek, L. Wei, J. Zhao, L.-J. Li, M. B. Chan-Park, Y. Yang, Y. Chen, Selective synthesis of (9,8) single walled carbon nanotubes on cobalt incorporated tud-1 catalysts. *J. Am. Chem. Soc.* **132**, 16747–16749 (2010).
8. W.-H. Chiang, R. Mohan Sankaran, Linking catalyst composition to chirality distributions of as-grown single-walled carbon nanotubes by tuning Ni_xFe_{1-x} nanoparticles. *Nat. Mater.* **8**, 882–886 (2009).
9. F. Yang, X. Wang, D. Zhang, J. Yang, D. Luo, Z. Xu, J. Wei, J.-Q. Wang, Z. Xu, F. Peng, X. Li, R. Li, Y. Li, M. Li, X. Bai, F. Ding, Y. Li, Chirality-specific growth of single-walled carbon nanotubes on solid alloy catalysts. *Nature* **510**, 522–524 (2014).
10. J. R. Sanchez-Valencia, T. Dienel, O. Gröning, I. Shorubalko, A. Mueller, M. Jansen, K. Amsharov, P. Ruffieux, R. Fasel, Controlled synthesis of single-chirality carbon nanotubes. *Nature* **512**, 61–64 (2014).
11. S. Zhang, L. Kang, X. Wang, L. Tong, L. Yang, Z. Wang, K. Qi, S. Deng, Q. Li, X. Bai, F. Ding, J. Zhang, Arrays of horizontal carbon nanotubes of controlled chirality grown using designed catalysts. *Nature* **543**, 234–238 (2017).
12. S. Helveg, C. Lopez-Cartes, J. Sehested, P. L. Hansen, B. S. Clausen, J. R. Rostrup-Nielsen, F. Abild-Pedersen, J. K. Nørskov, Atomic-scale imaging of carbon nanofibre growth. *Nature* **427**, 426–429 (2004).
13. S. Reich, L. Li, J. Robertson, Control the chirality of carbon nanotubes by epitaxial growth. *Chem. Phys. Lett.* **421**, 469–472 (2006).
14. X. Feng, S. W. Chee, R. Sharma, K. Liu, X. Xie, Q. Li, S. Fan, K. Jiang, In situ tem observation of the gasification and growth of carbon nanotubes using iron catalysts. *Nano Res.* **4**, 767–779 (2011).
15. J. Wang, P. Liu, B. Xia, H. Wei, Y. Wei, Y. Wu, K. Liu, L. Zhang, J. Wang, Q. Li, S. Fan, K. Jiang, Observation of charge generation and transfer during cvd growth of carbon nanotubes. *Nano Lett.* **16**, 4102–4109 (2016).

16. B. Liu, D.-M. Tang, C. Sun, C. Liu, W. Ren, F. Li, W.-J. Yu, L.-C. Yin, L. Zhang, C. Jiang, H.-M. Cheng, Importance of oxygen in the metal-free catalytic growth of single-walled carbon nanotubes from SiO_x by a vapor–solid–solid mechanism. *J. Am. Chem. Soc.* **133**, 197–199 (2010).
17. A. R. Harutyunyan, G. Chen, T. M. Paronyan, E. M. Pigos, O. A. Kuznetsov, K. Hewaparakrama, S. M. Kim, D. Zakharov, E. A. Stach, G. U. Sumanasekera, Preferential growth of single-walled carbon nanotubes with metallic conductivity. *Science* **326**, 116–120 (2009).
18. A. R. Harutyunyan, N. Awasthi, A. Jiang, W. Setyawan, E. Mora, T. Tokune, K. Bolton, S. Curtarolo, Reduced carbon solubility in fe nanoclusters and implications for the growth of single-walled carbon nanotubes. *Phys. Rev. Lett.* **100**, 195502 (2008).
19. S. Talapatra, S. Kar, S. K. Pal, R. Vajtai, L. Ci, P. Victor, M. M. Shaijumon, S. Kaur, O. Nalamasu, P. M. Ajayan, Direct growth of aligned carbon nanotubes on bulk metals. *Nat. Nanotechnol.* **1**, 112–116 (2006).
20. R. Rao, D. Liptak, T. Cherukuri, B. I. Yakobson, B. Maruyama, In situ evidence for chirality-dependent growth rates of individual carbon nanotubes. *Nat. Mater.* **11**, 213–216 (2012).
21. P. B. Amama, C. L. Pint, L. McJilton, S. M. Kim, E. A. Stach, P. T. Murray, R. H. Hauge, B. Maruyama, Role of water in super growth of single-walled carbon nanotube carpets. *Nano Lett.* **9**, 44–49 (2009).
22. F. Ding, A. R. Harutyunyan, B. I. Yakobson, Dislocation theory of chirality-controlled nanotube growth. *Proc. Natl. Acad. Sci. U.S.A.* **106**, 2506–2509 (2009).
23. V. I. Artyukhov, E. S. Penev, B. I. Yakobson, Why nanotubes grow chiral? *Nat. Commun.* **5**, 4892 (2014).
24. F. Yang, X. Wang, D. Zhang, K. Qi, J. Yang, Z. Xu, M. Li, X. Zhao, X. Bai, Y. Li, Growing zigzag (16, 0) carbon nanotubes with structure-defined catalysts. *J. Am. Chem. Soc.* **137**, 8688–8691 (2015).
25. M. He, Y. Magnin, H. Amara, H. Jiang, H. Cui, F. Fossard, A. Castan, E. Kauppinen, A. Loiseau, C. Bichara, Linking growth mode to lengths of single-walled carbon nanotubes. *Carbon* **113**, 231–236 (2017).
26. T. Inoue, D. Hasegawa, S. Chiashi, S. Maruyama, Chirality analysis of horizontally aligned single-walled carbon nanotubes: Decoupling populations and lengths. *J. Mater. Chem. A* **3**, 15119–15123 (2015).
27. Q. Yuan, H. Hu, F. Ding, Threshold barrier of carbon nanotube growth. *Phys. Rev. Lett.* **107**, 156101 (2011).
28. Y. Magnin, H. Amara, F. Ducastelle, A. Loiseau, C. Bichara, Entropy-driven stability of chiral single-walled carbon nanotubes. *Science* **362**, 212–215 (2018).
29. Z. Xu, L. Qiu, F. Ding, The kinetics of chirality assignment in catalytic single-walled carbon nanotube growth and the routes towards selective growth. *Chem. Sci.* **9**, 3056–3061 (2018).
30. G. Zhang, D. Mann, L. Zhang, A. Javey, Y. Li, E. Yenilmez, Q. Wang, J. P. McVittie, Y. Nishi, J. Gibbons, H. Dai, Ultra-high-yield growth of vertical single-walled carbon nanotubes: Hidden roles of hydrogen and oxygen. *Proc. Natl. Acad. Sci. U.S.A.* **102**, 16141–16145 (2005).
31. K. Hata, D. N. Futaba, K. Mizuno, T. Namai, M. Yumura, S. Iijima, Water-assisted highly efficient synthesis of impurity-free single-walled carbon nanotubes. *Science* **306**, 1362–1364 (2004).
32. J. Huang, Q. Zhang, M. Zhao, F. Wei, Process intensification by CO_2 for high quality carbon nanotube forest growth: Double-walled carbon nanotube convexity or single-walled carbon nanotube bowls? *Nano Res.* **2**, 872 (2009).
33. K. Bladh, L. Falk, F. Rohmund, On the iron-catalysed growth of single-walled carbon nanotubes and encapsulated metal particles in the gas phase. *Appl. Phys. A* **70**, 317–322 (2000).
34. J. H. Hafner, M. J. Bronikowski, B. R. Azamian, P. Nikolaev, A. G. Rinzler, D. T. Colbert, K. A. Smith, R. E. Smalley, Catalytic growth of single-wall carbon nanotubes from metal particles. *Chem. Phys. Lett.* **296**, 195–202 (1998).
35. L. Zhang, M. He, T. W. Hansen, J. Kling, H. Jiang, E. I. Kauppinen, A. Loiseau, J. B. Wagner, Growth termination and multiple nucleation of single-wall carbon nanotubes evidenced by in situ transmission electron microscopy. *ACS Nano* **11**, 4483–4493 (2017).
36. M. He, H. Jiang, I. Kauppi, P. V. Fedotov, A. I. Chernov, E. D. Obraztsova, F. Cavalca, J. B. Wagner, T. W. Hansen, J. Sainio, E. Sairanen, J. Lehtonen, E. I. Kauppinen, Insights into chirality distributions of single-walled carbon nanotubes grown on different $Co_xMg_{1-x}O$ solid solutions. *J. Mater. Chem. A* **2**, 5883–5889 (2014).
37. X. Wang, F. Ding, How a solid catalyst determines the chirality of the single-wall carbon nanotube grown on it. *J. Phys. Chem. Lett.* **10**, 735–741 (2019).
38. M. He, T. Yang, D. Shang, B. Xin, A. I. Chernov, E. D. Obraztsova, J. Sainio, N. Wei, H. Cui, H. Jiang, High temperature growth of single-walled carbon nanotubes with a narrow chirality distribution by tip-growth mode. *Chem. Eng. J.* **341**, 344–350 (2018).
39. M. He, A. I. Chernov, P. V. Fedotov, E. D. Obraztsova, E. Rikkinen, Z. Zhu, J. Sainio, H. Jiang, A. G. Nasibulin, E. I. Kauppinen, M. Niemela, A. O. I. Krause, Selective growth of swnts on partially reduced monometallic cobalt catalyst. *Chem. Commun.* **47**, 1219–1221 (2011).
40. H. Jiang, A. G. Nasibulin, D. P. Brown, E. I. Kauppinen, Unambiguous atomic structural determination of single-walled carbon nanotubes by electron diffraction. *Carbon* **45**, 662–667 (2007).
41. M. S. He, Z. W. Xu, D. H. Shang, X. Y. Zhang, H. Zhang, D. Li, H. Jiang, E. Kauppinen, F. Ding, Is there chiral correlation between graphitic layers in double-wall carbon nanotubes? *Carbon* **144**, 147–151 (2019).

Acknowledgments: We thank H. Amara, C. Bichara, A. Loiseau, K. Kanervo, and J. Kanervo for the helpful discussions. The usage of IBS-CMCM high performance computing system, Cimulator, is also acknowledged. **Funding:** We would like to acknowledge the National Natural Science Foundation of China (no. 51972184) and funding from Taishan Scholar Advantage and Characteristic Discipline Team of Eco Chemical Process and Technology. The authors also acknowledge support from the Institute for Basic Science (IBS-R019-D1), South Korea. **Author contributions:** M.H., F.D., and J.Z. conceived and designed the work. M.H., H.J., and F.C. performed the in situ ETEM experiment. F.D. and X.W. proposed the theoretical model. S.Z. and J.Z. carried out the Raman characterization. All authors discussed the results, compiled the figures, and cowrote the manuscript. **Competing interests:** All authors declare that they have no competing interests. **Data and materials availability:** All data needed to evaluate the conclusions in the paper are present in the paper and/or the Supplementary Materials. Additional data related to this paper may be requested from the authors.

Submitted 6 November 2018
Accepted 22 October 2019
Published 13 December 2019
10.1126/sciadv.aav9668

Citation: M. He, X. Wang, S. Zhang, H. Jiang, F. Cavalca, H. Cui, J. B. Wagner, T. W. Hansen, E. Kauppinen, J. Zhang, F. Ding, Growth kinetics of single-walled carbon nanotubes with a (2*n*, *n*) chirality selection. *Sci. Adv.* **5**, eaav9668 (2019).